### Title
Phytoplankton blooms associated with upwelling at Cabo Catoche




### Journal
Continental Shelf Research, 174(Water. Air. Soil Pollut. 218 2011)

### ISSN
0278-4343



### Authors
Reyes-Mendoza, Oscar
Herrera-Silveira, Jorge
Mariño-Tapia, Ismael
et al.



### Publication Date
2019-02-01

### DOI
10.1016/j.csr.2018.12.015

Peer reviewed

Continental Shelf Research 174 (2019) 118–131

Contents lists available at ScienceDirect

Continental Shelf Research

journal homepage: www.elsevier.com/locate/csr

Research papers

# Phytoplankton blooms associated with upwelling at Cabo Catoche

Oscar Reyes-Mendoza[a,b,*], Jorge Herrera-Silveira[c], Ismael Mariño-Tapia[c], Cecilia Enriquez[a], John L. Largier[d]

[a] Facultad de Ciencias, Unidad Académica Yucatán, Universidad Nacional Autónoma de México, Sisal, Yucatán, C.P. 97356, México
[b] Posgrado en Ciencias del Mar y Limnología, Universidad Nacional Autónoma de México, Av. Ciudad Universitaria 3000, C.P. 04510 Coyoacán, Ciudad de México, Mexico
[c] Departamento de Recursos del Mar, Centro de Investigación y de Estudios Avanzados del Instituto Politécnico Nacional, Mérida, Yucatán C.P. 97310, Mexico
[d] Bodega Marine Laboratory, University of California Davis, Bodega Bay, CA 94923, USA

ARTICLE INFO

*Keywords:*
Yucatan Upwelling
Yucatan continental shelf
Hydrography
Slope water intrusion
Flow nutrients
Bio-productivity

ABSTRACT

In this work, the spatial and temporal implications of the Non-Eastern Boundary Upwelling (Non-EBUS) on the bio-productivity from coastal shallow waters have been studied. At the coast of Cabo Catoche, on the Yucatán shelf, two 12-day field campaigns (April and July) were conducted. Cross-shore CTD-fluorescence profiles, water samples, and plankton were collected each day. Nutrients, ocean temperature and currents times series from two moorings (8 and 12 m depth) were analyzed, as were temperature and chlorophyll (Chl-a) from satellite data. The water masses from the Yucatan channel reached the coast of Cabo Catoche in both study periods. The Yucatan Upwelling Water (YUW, ~ 19.6–22.5 °C) supplied the surface and subsurface water, up to 6 km offshore, with nutrients during the upwelling pulses from 2 to 5 days. Nutrients were higher in April (nitrate, ammonium < 5, 18 μmol $L^{-1}$), but the phytoplankton bloom was more consistent in July (Chl-a mean, 1.45 mg $m^{-3}$) showing greater distribution across the coast. The steady upwelling plume (cold water, high nutrients) recorded in Cabo Catoche and observed on the north shelf, could have been the result of dynamic uplift in the Yucatan Channel prior to the field campaign. Through the way to the shelf, the plankton increased, explaining the high temporal association between low temperatures and the phytoplankton bloom at the coast. The Non-EBUS has strong implications for the pelagic ecosystem from Cabo Catoche, enhancing productivity and triggering energy flow by the physical process.

## 1. Introduction

Phytoplankton blooms are often associated with the classical wind-driven coastal upwelling process that brings new nutrients to the photic zone which are assimilated by plankton (Chavez and Messié, 2009). In Non-Eastern Boundary regions, the physical upwelling process can also be driven by flow-topography interactions including bottom Ekman layer transport, flow separation, and vorticity conservation (Tomczak and Godfrey, 1994; Simpson and Sharples, 2012). In Non-Eastern Boundary Upwelling Systems (Non-EBUs) the term uplift is used to refer to the raising of cold water and nutrients towards, but not reaching, the surface, and the term upwelling to the raising of nutrients to the surface, while, the term slope water intrusion is used to describe the uplift of slope water adjacent to the continental slope to a shallower depth on the upper continental slope or shelf (Roughan and Middleton, 2002). However, in both physical systems, EBUS and Non-EBUS, the phytoplankton blooms are associated with the water which rises from the bottom (Coelho-souza et al., 2012).

Between March-August, Non-EBU processes are reported around the southeast of the Yucatan continental shelf sea (YS) at the northeastern corner of the Yucatan Peninsula, (Cochrane, 1968; Furnas and Smayda, 1987; Merino, 1997). These processes could be considered the result of water uplift and slope water intrusion from the Yucatan channel along isopycnal surfaces beneath the thermocline onto the Yucatan shelf (Furnas and Smayda, 1987; Jouanno et al., 2018). Around Cabo Catoche coast the cold water reaches the surface and then sinks, moving out to the northwestern YS (Alacranes reef, *see* Fig. 1) forming a dome (Merino, 1992). The upwelling water masses present on the Yucatan Shelf are Subtropical Under Water (SUW) from the Yucatan channel (~ 300 m depth), Caribbean Surface Water (< 100 m depth) and between them is the Yucatan Upwelled Water (YUW), (Merino, 1992; Carrillo et al., 2016).

* Corresponding author at: Facultad de Ciencias, Unidad Académica Yucatán, Universidad Nacional Autónoma de México, Sisal, Yucatán, C.P. 97356, México.
*E-mail addresses:* bioskar@yahoo.com.mx (O. Reyes-Mendoza), jherrera@cinvestav.mx (J. Herrera-Silveira), imarino@cinvestav.mx (I. Mariño-Tapia), cenriquez@ciencias.unam.mx (C. Enriquez), jlargier@ucdavis.edu (J.L. Largier).

https://doi.org/10.1016/j.csr.2018.12.015
Received 5 June 2018; Received in revised form 22 December 2018; Accepted 31 December 2018
Available online 11 January 2019
0278-4343/ 

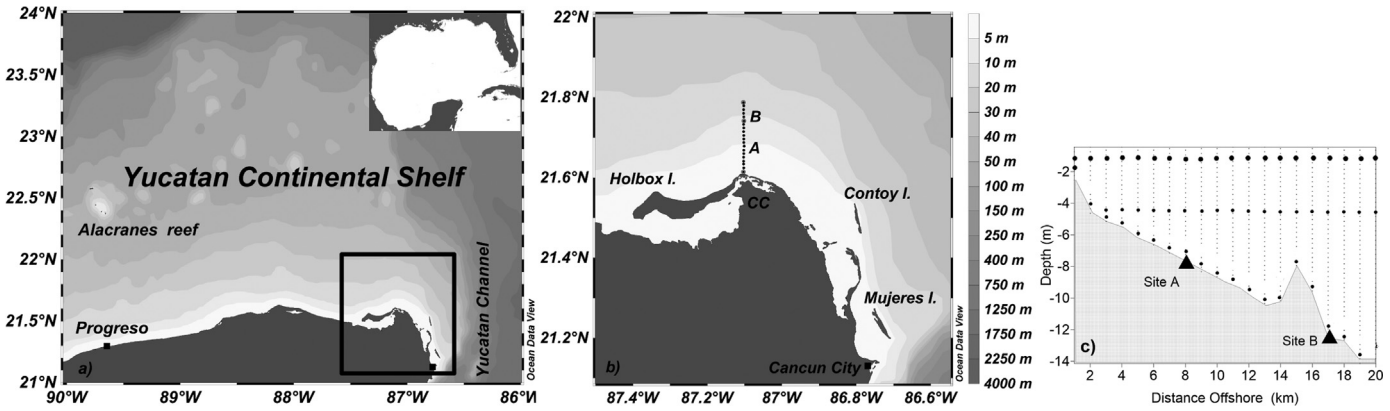


**Fig. 1.** a) Yucatan shelf and study site in the northeast of the Yucatan Peninsula, Mexico, b) cross-shore transect (north-south) and collecting sites A and B, c) points of collecting and measuring at the surface (at 0.5 m depth), mid-layer (5 m depth) and the bottom (1 m before the seafloor).

The YUW is classified by temperatures between 16 °C and 22.5 °C, and salinities between 36.1 psu and 36.6 psu. Nutrients range from 6 to 17 μmol $L^{-1}$ for nitrate, 1.2 to 1.7 μmol $L^{-1}$ for phosphate, and 4.5 to 7.3 μmol $L^{-1}$ for silicate (Furnas and Smayda, 1987; Merino, 1992). In Cabo – Catoche (CC) shallow waters (~ 12 m depth), Reyes-Mendoza et al. (2016) reported periodic slope water intrusions (7–21 days, T < 22.5 °C) associated with YUW, with greater slope water intrusion around spring-summer than fall-winter, which seems to described by Merino (1997) and Ruiz-Castillo et al. (2016) to all the continental shelf sea of Yucatan-Peninsula

In association with the upwelling waters (YUW), Cabo Catoche has been reported as the most important region (Licea et al., 2017) in terms of biological productivity on the Yucatan Shelf, with a high concentration of Chlorophyll - a (up to 1.7 mg $m^{-3}$), and a large abundance of phytoplankton (up to 734,000 cell/l) and species (~ 175 species). About that, an association between low temperature (< 22.5 °C) and high Chlorophyll - a (> 1 mg $m^{-3}$) has also been reported using satellite images, (Salmerón-García et al., 2011; Cerdeira-Estrada and López-Saldaña, 2011). The occurrence of harmful algal blooms (HABs) associated with waters from the Yucatan channel (Enriquez et al., 2010), generated by dinoflagellates *Scrippsiella trochoidea, Prorocentrum* sp. and diatoms *Cylindrotheca closterium, Nitzschia longissimi* among others, is a regular phenomenon on the north coast of the Yucatan Peninsula. This has strong implications for the trophic web of the pelagic ecosystem and artisanal fisheries (Merino-Virgilio et al., 2014). Finally, this productivity is linked to high biodiversity in the Cabo Catoche region composed of numerous fish species, octopus, turtles, manta rays and whale shark populations, which are exploited by fisheries and ecotourism industries (Piñeiro et al., 2001; Ardisson et al., 2011; Ramírez-Macías et al., 2012; Cárdenas-Palomo et al., 2015).

We believe, that the slope water intrusion pulses create phytoplankton bloom events that last for a period of days and occur over an area of several kilometers, which develop downstream of the upwelling center at Cabo Catoche and the shelf-edge upwelling along the eastern boundary of the Yucatan Shelf. This is similar to Agulhas Bank in South Africa (Mitchell-Innes et al., 1999), the East China Sea, east of Taiwan (Gong et al., 2000), the Brazilian coast, south of Cabo Frio (Pereira Brandini et al., 2013) and the Australian coast, south of Smoky Cape (Roughan et al., 2003).

Our aim in this study was to characterize the spatial and temporal interaction between physical, chemical and biological upwelling processes in shallow water at Cabo Catoche. This interaction is key to understanding ecosystem function; therefore, it is necessary to study the processes step by step since they may occur only in a few days and could be ephemeral processes. As a preliminary exploration of this idea, we conducted two 12-day surveys along a south-north transect of Cabo Catoche (coastal waters, ~ 2–13 m depth). We expected to see the influence of upwelled water (cold, high-nutrient, and/or high-Chlorophyll) on the phytoplankton bloom around the coast (~ 20 km offshore). Our first survey was in April 2012 and the second survey was in July 2012, both during the established upwelling season (Cochrane, 1968; Furnas and Smayda, 1987; Merino, 1997).

## 2. Material and methods

### 2.1. Study area

The study area (Fig. 1) is the coast of Cabo Catoche (21.50–21.85°N, at 87.1° W), between the 2 and 15 m isobaths, around 20 km offshore, in the Caribbean Mesoamerican Shelf-Ecoregion (Lara-Lara, 2008). The Caribbean winds are dominant from the east and southeast (Pérez-Santos et al., 2010). Data from the national meteorological service (SMN-CONAGUA, period: 1951–2010) indicate that the annual-averaged air temperature in the region is 26.4 °C with a monthly maximum in May (38.6 °C). There are three climatic seasons: the dry season, from March to May (0–60 mm of rain on average), when the winds from ESE and SE are more common (mean 18–20 km/h); the rainy season, from June to October (> 110 mm of rain, wind, mean 15–20 km/h) – this season is characterized by the occurrence of tropical storms and Hurricanes; and the northerly season, from November to February – this season is characterized by strong frequently northerly winds (50–90 km/h) and low air temperatures associated with polar fronts crossing the Gulf of Mexico (Medina-Gómez and Herrera-Silveira, 2006). Over the Yucatan continental shelf, these northerly winds (known colloquially as “Los Nortes”) have the capacity to affect the ocean-atmosphere heat fluxes, reducing oceanic heat (Hernández-Téllez et al., 1993, Zavala-Hidalgo et al., 2014). Nutrient concentrations of 0.7–16.5 μmol $L^{-1}$ nitrate, 0.5–38.4 μmol $L^{-1}$ ammonium, 0.1–2.4 μmol $L^{-1}$ phosphate, and 2.6–37.8 μmol $L^{-1}$ silicate have been reported (Cárdenas-Palomo, 2007; Cárdenas-Palomo et al., 2015; Reyes-Mendoza, 2010). Chlorophyll-a concentrations (Chl-a) have been reported from 0.5 to 6.6 mg $m^{-3}$ and zooplankton biomass between 37 and 222 mg $m^{-3}$.

### 2.2. Fieldwork

From April to August 2012, an acoustic profiler (AWAC-Nortek) was anchored 12 km offshore, at 8 m depth (site A), and another 17 km offshore (Site B) at 12 m depth, both recording currents (m $s^{-1}$), sea level (m) and temperature (ºC) every 10 min (Fig. 1b, c). Wind data correspond to the Jacques-Yves Cousteau Coastal Observatory, (21°20′8″ N and 89°18′25″ W), granted by David Valdes from CINVESTAV-IPN.

Two field campaigns were performed during 12 continuous days, in

April (2–13, dry season) and another in July 2012 (18–29, rainy season). Every day profiles were taken at twenty stations along a cross-shore transect (Fig. 1b, c) using a CTD Sea-Bird 19 plus at a sampling frequency of 4 Hz to record: temperature (° C); salinity (psu) and density (Sigma-Theta kg m$^{-3}$); fluorescence, corresponding to Chl-a (mg m$^{-3}$), and turbidity (NTU) were measured with a WetLabs Fluorimeter (ECO - FL-NTU) attached to the CTD.

At sites A and B, during each day of the campaign, a Secchi disk depth reading was performed (Holmes, 1970). At the same depths and at the sea surface 1 L of water was collected with a Van Dorn Bottle and preserved at 4 °C until its analysis. Zooplankton samples were simultaneously collected by towing a conic net of 300 μm, Ø 0.30 m and were fixed in formaldehyde with Borate Sodium and seawater (UNESCO, 1979; Cadena-Ramírez, 2013a, 2013b); the net was ballasted to collect the sub-water sample (*Sechii* depth).

### 2.3. Laboratory analysis

Each water sample was filtered with nitrocellulose filters (0.45 μm pore, Millipore); these filters were dissolved to determine Chl-a using 90% acetone as a solvent and later analyzed spectrophotometrically following the technique described by Parsons et al. (1984). The filtered water was used to quantify nutrients by spectrophotometry, following the method described by Strickland and Parsons (1972). The indophenol blue method was used to quantify Ammonium ($NH_4^+$) content, and Nitrite ($NO_2^-$) was determined by a reaction with sulphanilamide and naphthyl-N in acid medium to form the diazo dye. Nitrate ($NO_3^+$), was determined via reduction to nitrite in a cadmium-copper column and was analyzed as nitrite. Phosphate ($PO_4^{3-}$) was determined using acidity molybdate and subsequent reduction with an ascorbic acid to measure its absorbance afterward. Finally, Silicate ($SiO_4^{4-}$) was estimated using the molybdic acid technique with methol– sulfite as the reducing agent. To determine zooplankton biomass, the wet-mass technique was used, and the results were expressed in mg m$^{-3}$ (Omori and Ikeda, 1984). All sampling was performed between 7:00 and 13:00 h local time.

### 2.4. Data analysis

#### 2.4.1. CTD Profilers

The downward CTD profile data were filtered, aligned and split with the Sea Bird Data-Processing software. Subsequently, a Gaussian interpolation was performed to create vertical distribution maps (Emery and Thomson, 1997) over time and for both stations (Figs. 4–7). The 22.5 °C isotherm was considered to represent the boundary between the Yucatan Upwelling Water (YUW) and Caribbean Surface Water (CSW) – this isotherm also represents the center of the Yucatan current thermocline and has previously been used as an indicator of upwelling water masses (Cochrane, 1968; Merino, 1992, 1997). Chl-a values determined by an in situ fluorometer attached to a CTD were highly correlated with Chl-a values extracted by the acetone method (R2 = 0.86); therefore Chl-a obtained by the CTD was used to construct distribution maps, due to the quantity of optical data.

#### 2.4.2. Satellite image

Contour maps for sea surface temperature (°C) and Chl-a concentrations (mg m$^{-3}$) were plotted with satellite data from NOAA Aqua Modis to NPP, 0.025°, 3-day composite, around April 5 and July 19, 2012.

#### 2.4.3. Currents and Progressive Vector Diagrams (PVD)

Progressive Vector Diagrams (PVDs) were plotted for the current velocity time-series recorded by the ADCP at sites A and B (surface at 0.5 m depth and bottom 1 m before the seafloor of each station), which present the vector sum of the individual vectors, plotting them head to tail for the period of interest. For this, time-integrated displacements along the two orthogonal directions ($x$, $y$) were calculated from the velocity components (*Ux*, east-west; *Uy*, north-south) to estimate a "pseudo" downstream displacement of a parcel of water from its origin ($x_0$, $y_0$) (Emery and Thomson, 1997). It was named "toward" to describe the flow of the currents in base to the PVD analysis. These analyses have been used to estimate transport in the coastal ocean from point measurements of velocity time series, despite the fact that they only strictly approximate true particle trajectories in regions where the currents are spatially uniform (Carlson et al., 2010). These PVDs were embedded over the contour maps of sea surface temperature (°C) and Chl-a concentrations (mg m$^{-3}$) from satellite data.

#### 2.4.4. Anomaly analysis of temperature and Chl-a

The values of temperature and Chl-a recorded and collected at the *Sechii* disk depth, on sites A and B were used to that analysis. Chl-a values extracted by the acetone method were used in this analysis. The anomaly is defined as the difference between the variable (temperature/Chl-a) collected at the *Sechii* depth and the long-term mean variable (take over the full-time series, n = 12 days). The Pearson coefficient was calculated for each analysis.

#### 2.4.5. Temporal analysis of nutrients, Chl-a and zooplankton biomass

The data of nutrient, Chl-a, and zooplankton were classified by upwelling (Up) and non-upwelling (Non-Up) days to each field campaign. Due to that these data did not fully satisfy the assumptions of normality, the statistical difference on the classification was evaluated by applying the non-parametric Kruskal-Wallis test and a box plot graphical analysis (Zar, 1999). The Chl-a values extracted by the acetone method were used in this analysis.

#### 2.4.6. Integration analysis of physical, chemical and biological components

In order to establish an association between physical, chemical and biological variables in sites A and B, multivariate analyzes were performed. A canonical redundancy analysis (RDA) was conducted with the software CANOCO 4. 5 recommended by Ter Braak and Smilauer (1998) and Lepš and Šmilaur (2003) for linear ordering methods. The variables collected at the surface (0.5 m depth) and *Sechii* depth were classified in the following way: temperature, salinity, and density as an independent; nutrients, chlorophyll-*a*, zooplankton biomass as dependents; and the sampling days (date) as covariates (*Dummies*). The Monte Carlo test (9999 permutations) was used to establish significant differences, in compulsory ordering models, with $p \leq 0.05$ value. The null hypothesis assumes that neither primary variable is dependent on the explanatory variables.

## 3. Results

The results are divided into temperature and wind during the upwelling season and currents during field campaigns; CTD cross-shore patterns (CTD); temperature and Chlorophyll-a satellite maps; chemical and biological temporal analysis; integration analysis of physical, chemical and biological components.

### 3.1. Temperature and wind time series

Throughout five months of recording, (upwelling season 2012) the temperature at site B dropped (< 22.5 °C) approximately 6 times (including the field campaign dates), indicating 6 possible upwelling events. The temperature time series (Fig. 2, a) from sites A and B, had a similar tendency with a correlation coefficient of 0.59 and an average difference of 2.29 °C ± 1.3 SD. Site A presented the maximum temperature (28.9 °C), while site B presented the minimum (19.6 °C). At the end of July and for half of August the temperature values were closer between sites, around 23–25 °C. The wind components (*Wx*, from east has a positive symbol and Wy, from north has positive symbol) were often positive from east and north (Fig. 2, b); the magnitude was

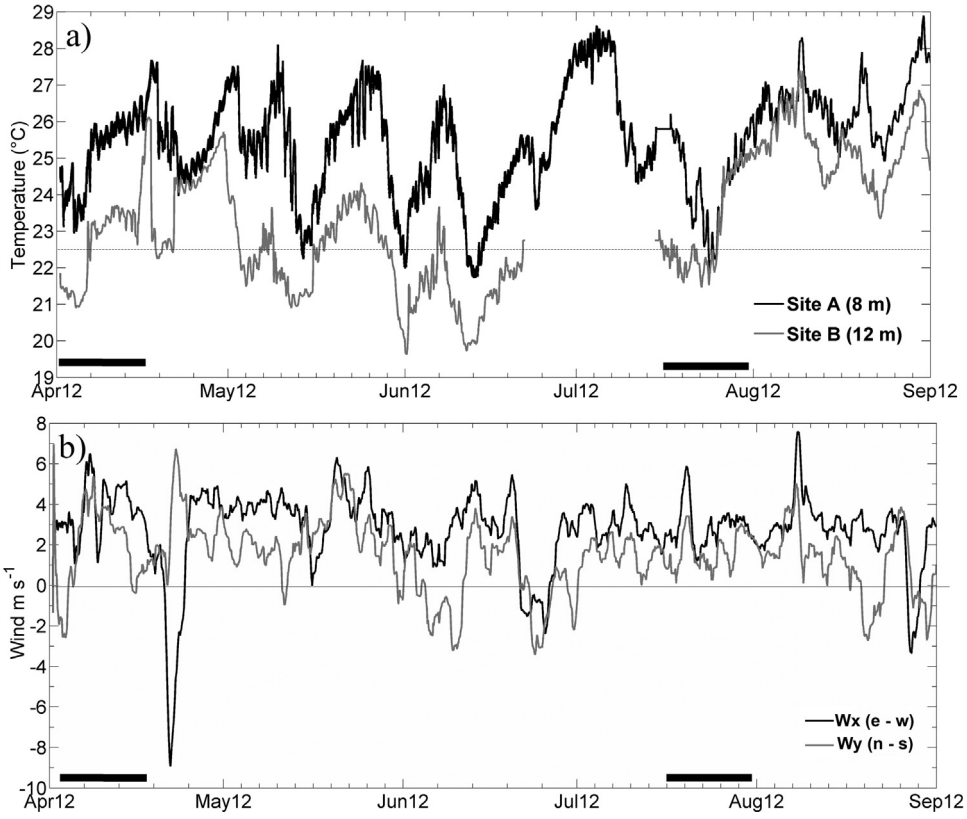


**Fig. 2.** a) Temperature time series from site A and site B during the 2012 upwelling season, field campaigns in April and July are indicated by a black line along the bottom of the figure, b) low pass filter (diurnal) of wind components *Wx* (from east positive) and *Wy* (from north positive).

characteristic of the region and season, with a maximum speed of 15.6 m s$^{-1}$, and an average and standard deviation (SD) of 4.4 ± 2.8 m s$^{-1}$.

### 3.1.1. Temperature and wind time series in the field campaigns

In April (Fig. 3a, borderline), at site A (8 m depth) an average temperature of 24.9 °C ± 0.94 was recorded, with a range of 22.9–26.3 °C. While site B (12 m depth) presented an average of 22.5 °C ± 1.01, and a range of 20.9–23.7 °C. In July (Fig. 2a) the average temperature at site A was 24 °C ± 1.09, with a range of 21.9–25.7 °C, and at site B (12 m depth) the average temperature was 22.8 °C ± 1.17, with a range of 21.4–25.1 °C.

From April 2 to 6 the temperature (Fig. 3a) at site B was below of 22.5 °C, that tendency also was at site A but without reach the upwelling reference value. The first four days of the April field campaign the wind (Fig. 3c) come constantly from the southeast, reaching around 4–6 m s$^{-1}$ until April 5, when in a couple of hours the wind abruptly changed of direction, now coming from north with gusts of 10 m s$^{-1}$ increasing, and increasing in magnitude, that was associated with a meteorological anomaly known colloquially as “Turbonadas” (squall)

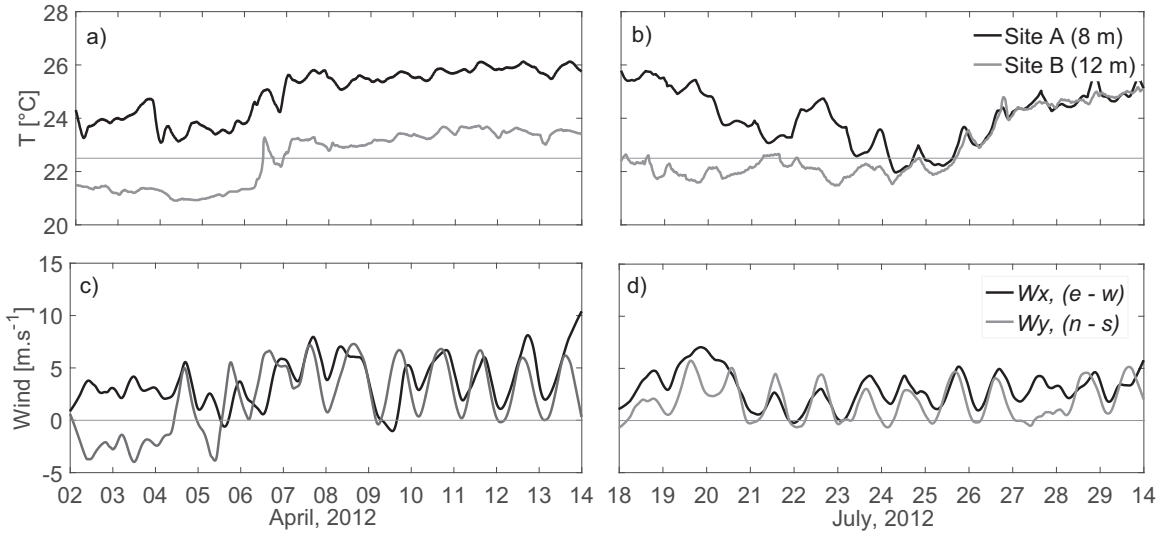


**Fig. 3.** Temperature time series from sites A and B during the field campaigns from April a) and July b), and low pass filter (diurnal) of wind components *Wx* (from east positive) and *Wy* (from north positive) from field campaigns from April a) and July b).

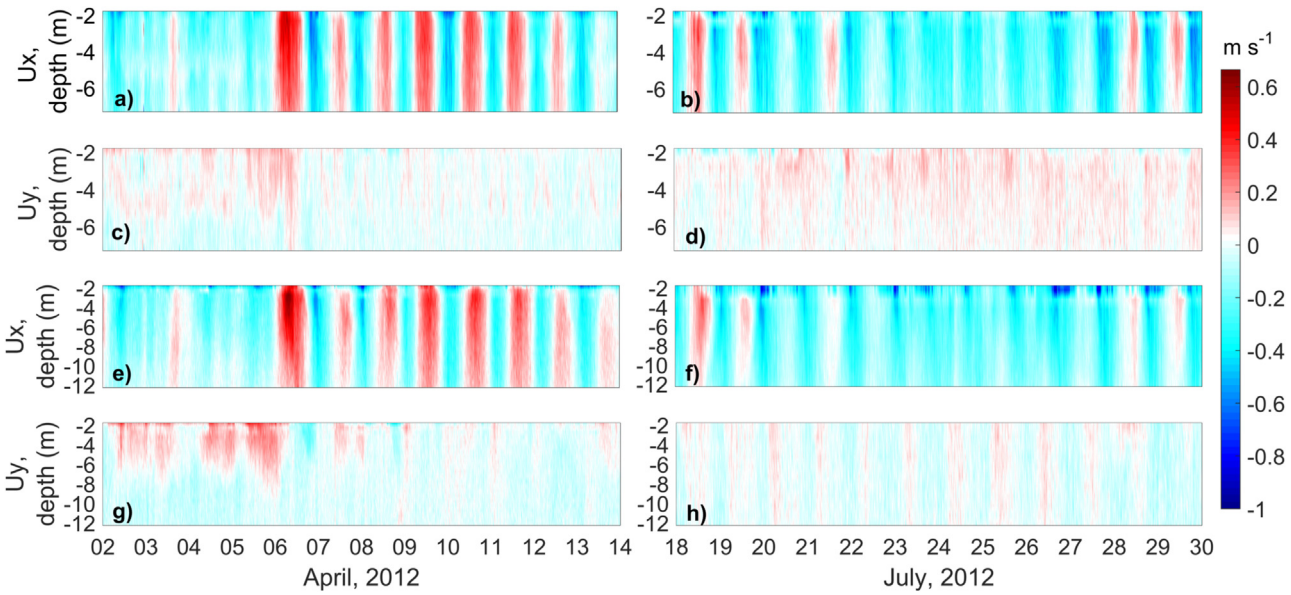


**Fig. 4.** Profile currents of the zonal component (*Ux*, toward east positive) and meridional component (*Uy*, toward north positive) at site A (a, c, e, g) and B (b, d, f, h) for each field campaign (April and July).

on the region. Working in the field was noted that the sea level increased along the beach as result of flooding generated by that wind. Around 6 h later the wind changed, now coming from the northeast, showing a normal pattern (east and diurnal northeast breeze) throughout the following few days.

From July 18 to 25 the temperature at site B was below 22.5 °C, the temperature in site A reach the upwelling reference value around day 24 (Fig. 3b). In the July field campaign, the wind direction (Fig. 3d) come from east and northeast, characteristic of the region's climate.

### 3.2. Currents times series in the field campaigns

The currents, as well as the wind, showed two kinds of variability throughout April field campaign. From April 2 to 6, the zonal current (*Ux*, toward east positive) in sites A and B (Fig. 4a, e, respectively) was constant toward west around $-0.2$ to $-0.6\,m\,s^{-1}$, even reaching $-1.1\,m\,s^{-1}$ at the surface layer and shows some diurnal alternations toward east, principally on April 3, when it reaches around $0.2\,m\,s^{-1}$. The meridional current (*Uy*, toward north positive, Fig. 4, c, g) showed shearing in the water column, the current surfaces layers (around 1.5–6 m depth) was traveling toward north with magnitude around 0.2–0.4 $m\,s^{-1}$, while the current bottom layer toward south around $-0.2$ to $-0.3\,m\,s^{-1}$. Onset April 6 at the end field campaign, the currents change these tendencies and showed semidiurnal alternations in its directions such zonal and meridional currents, more evident on zonal where reach magnitude maximum around $0.6\,m\,s^{-1}$. The sea temperature, wind, and currents showed a stretch relationship between them around this first period.

In July field campaign (Fig. 4, b, d, f, h), the currents had a similar temporal tendency to weakening its diurnal and semidiurnal alternations associated to low temperature, principally around July 23–27. The zonal dominant current (Fig. 4, b, f), in these days was toward west around $-0.4$ to $-0.5\,m\,s^{-1}$, and the zonal current (Fig. 4, d, h) was not clearly dominant, with average of $0.3\,m\,s^{-1}$ (toward north) and $-0.3\,m\,s^{-1}$ (toward south) in site A and B respectively. However, did not show sheering at the water column, and the magnitude recorded was lower than Abril in zonal and meridional currents.

### 3.3. Cross-shore distribution of the water masses

The water masses along CC coast are a mixture of the deep-water masses present in the Yucatan Channel and the Gulf of Mexico. In both field campaigns, the following were recorded: the Caribbean Surface Water (CSW), North Atlantic Subtropical Underwater (SUW), and the Yucatan Upwelling Water (YUW). The YUW presented a temperature between 20.8 and 22.5 °C, salinity around 36.2 and 36.5, and density of 25 and 25.75 $kg\,m^{-3}$. A statistical summary for all profile data is shown in Table 1 as a reference.

During each campaign, two spatial-temporal scenarios were characterized, upwelling and not-upwelling. While the uplift was identified a gradient cross-shore was confirmed by upwelling waters (YUW) and Caribbean surface water masses (CSW) in Cabo Catoche waters.

Around April 2–5, the upwelling scenario was characterized by the presence of the YUW, cold (< 22.5 °C, Fig. 5a, e, i) and dense water (> 25 $kg\,m^{-3}$, Fig. 5c, g, k) covering the coast from 12 km to beyond 20 km offshore and reaching the surface around 14–17 km (over the bathymetric peak, *see* Fig. 1c). The not-upwelling scenario was from April 6 to April 13, when warm (> 23 °C, Fig. 5c, d) and less dense water (> 25 $kg\,m^{-3}$, Fig. 5g, h) was present. The salinity showed widespread dispersion cross-shore with no clear pattern (Fig. 5b, f, j). Turbidity values > 2 NTU were observed in all water column between 1 and 8 km offshore during days 5–7 and 9–10 (Fig. 5d, h, l), and was higher in all transect at the bottom layer on day 6, except for 15 km offshore, where is a peak in the bathymetry (Fig. 1b, c), this turbidity was due to the sediment suspension generate by the squall (recorded on April 5). A nearshore is defined as 1–8 km from the coast, where the water was always warmer, had a lower salinity, lower chlorophyll, and more turbidity. Furthermore, the water was typically mixed with a top-

**Table 1**
Statistics values for CTD profiles during field campaigns.

| | | T °C | Sal (PSU) | ST ($kg\,m^{-3}$) | Chll-a ($mg\,m^{-3}$) | Turbidity (NTU) |
|---|---|---|---|---|---|---|
| April | Mean | 24.1 | 36.36 | 24.63 | 0.86 | 1.17 |
| | SD | 1.62 | 0.12 | 0.54 | 1.57 | 0.86 |
| | Min | 20.81 | 35.1 | 22.28 | 0.01 | 0.06 |
| | Max | 30.32 | 36.92 | 25.83 | 11.9 | 18.42 |
| July | Mean | 24.16 | 36.39 | 24.65 | 1.45 | 1.09 |
| | SD | 1.74 | 0.15 | 0.58 | 1.2 | 0.49 |
| | Min | 21.24 | 35.42 | 22.21 | 0.01 | 0.39 |
| | Max | 30.89 | 37 | 26 | 5.31 | 8.49 |

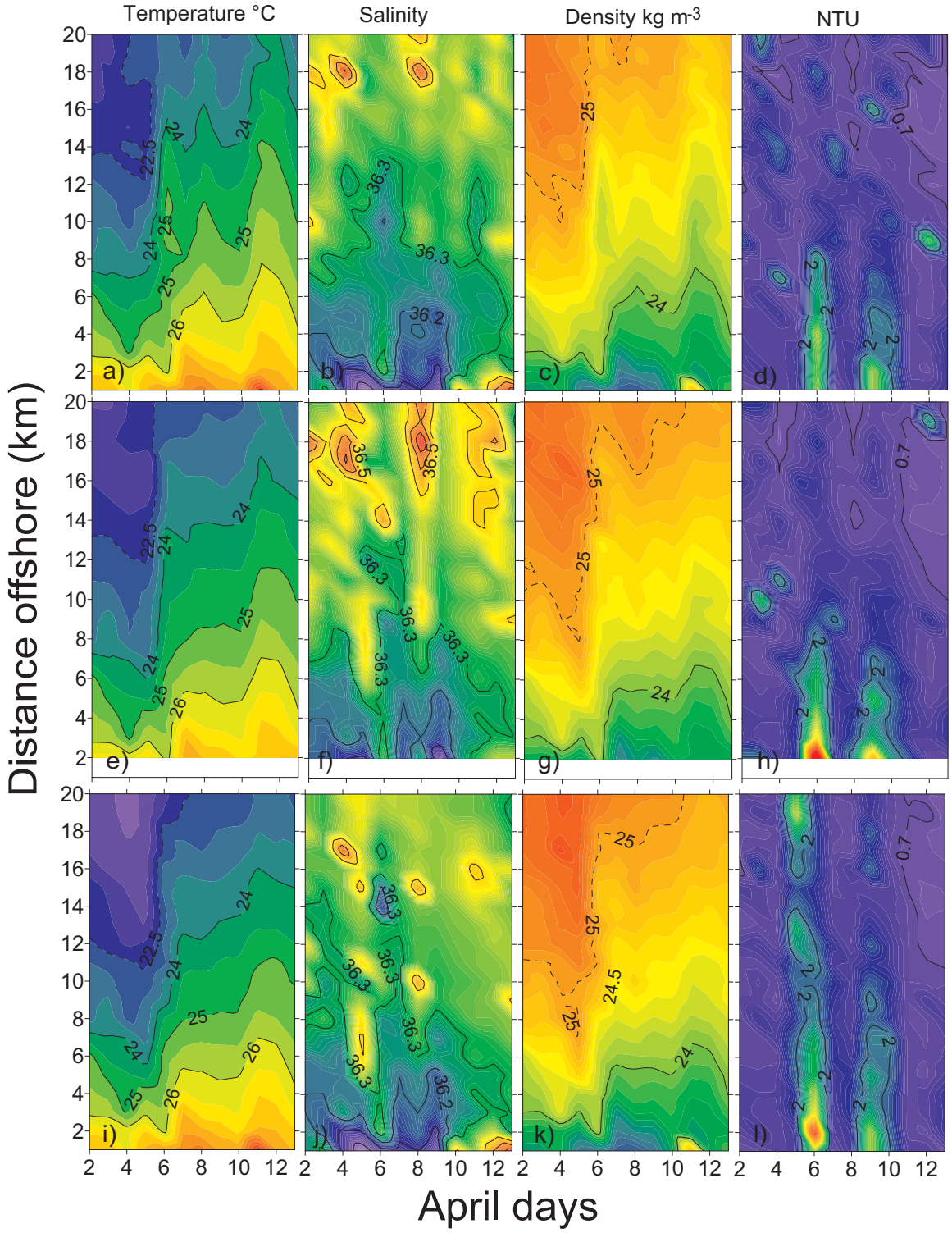


**Fig. 5.** Space-time diagram of environmental variables for data near the surface (0.5 m depth, a–d), mid layer (5 m depth, e–h), and near the bottom (1 m above the seafloor, i–l), April.

bottom density difference less than 0.1 kg m$^{-3}$ and *Secchi* disk depth of 5 m which was typically less than bottom depth nearshore (around the 6 m isobath).

In July, the upwelling scenario was around July 18–24, the YUW was closer to the coast than in April and the water scarcely reached the surface (Fig. 6). In upwelling days, the cold water (< 23 °C) was present at the bottom as of 5–6 km offshore, and nearshore, within 6 km of the coast, was always warmer with lower salinity (Fig. 6a, e, i). On July 18–19, the cold water reached the surface (-2 m, *see* Fig. 1c) around 18 to ≤ 20 km, while on July 23–24 it was closer to coast, around 7–8 km (Fig. 6a, e, i). The cold water showed a broader distribution at the bottom, and mid layer than at the surface, it came into the coast twice, on July 20 and 24, around 13 km and 6 km respectively. During this period, the minimum temperature (21.2 °C) was recorded offshore. Salinity values (Fig. 6b, f, g) of 36.5 and 37 were presented offshore (> 6 km) at the surface and at the bottom (*see* Fig. 1c). Dense water was

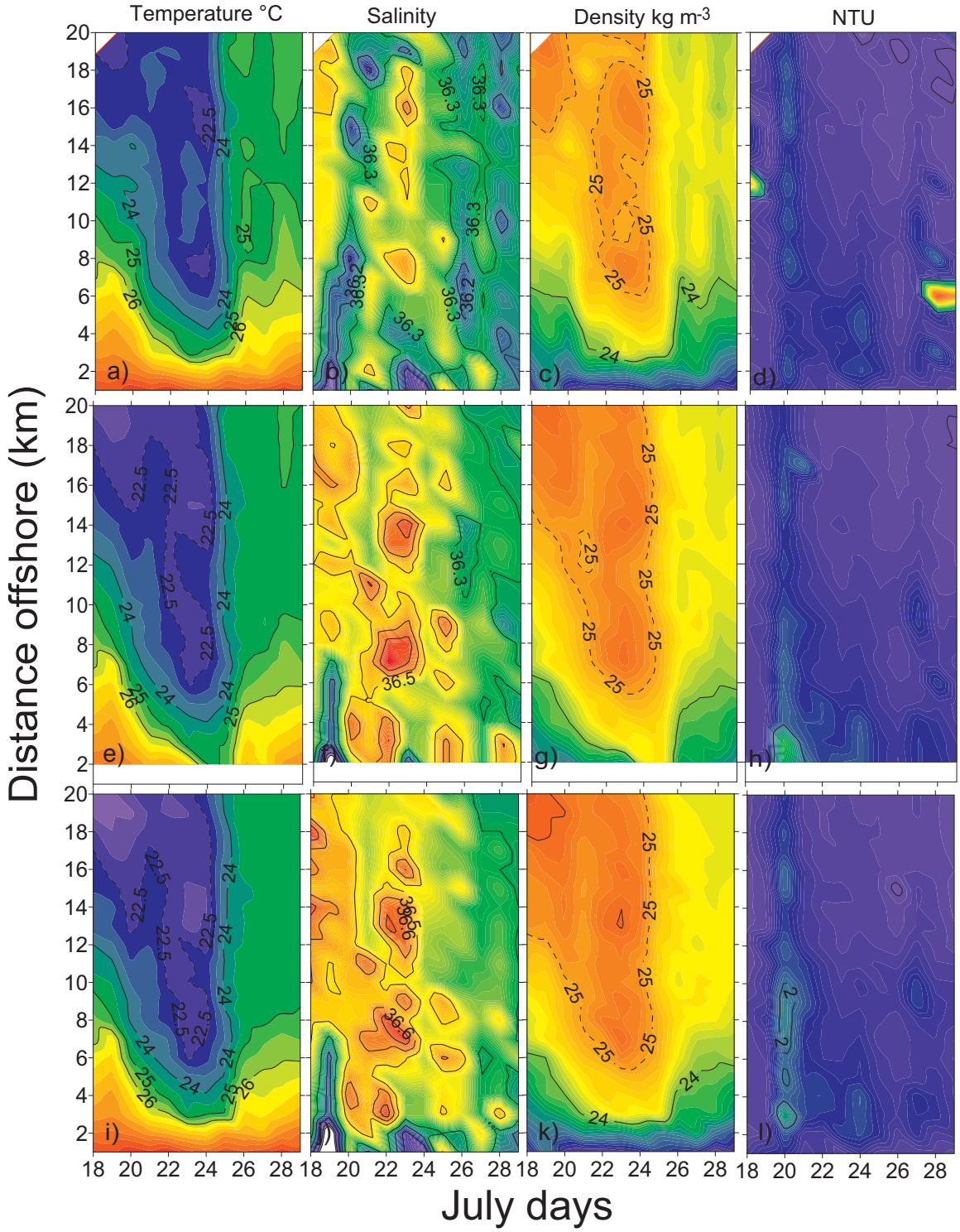


**Fig. 6.** Space-time diagram of environmental variables for data near the surface (0.5 m depth, a–d), mid layer (5 m depth, e–h), and near the bottom (1 m above the seafloor, i–l), July.

widely distributed along the bottom, reaching 6 km offshore on July 23 and 24 (Fig. 6c, g, k). Turbidity values had lower variability and lower values in July than in April. Unlike the other variables, turbidity (Fig. d, h, l) did not show a correlation with the presence of YUW. The not-upwelling scenario (July 25–28) showed a homogeneous water column with warm water ($> 23\,^{\circ}C$, Fig. 6c, d) and less dense water ($< 25\,kg\,m^{-3}$, Fig. 6g, h).

### 3.4. Satellite data and currents during the field campaigns

By plotting satellite data (Fig. 7) it was possible to observe a steady upwelling plume (Temperature and Chl-a) at the surface. In April (April 5, three day-composite) the lowest SST was $\sim 23.5\,^{\circ}C$ (gray) and Chl-a was high $\sim 1.2\,mg\,m^{-3}$, while July (July 19, three day-composite) showed higher surface Chl-a than April, reaching almost $11\,mg\,m^{-3}$, and temperatures $\sim 26\,^{\circ}C$. In each field campaign, it was possible to

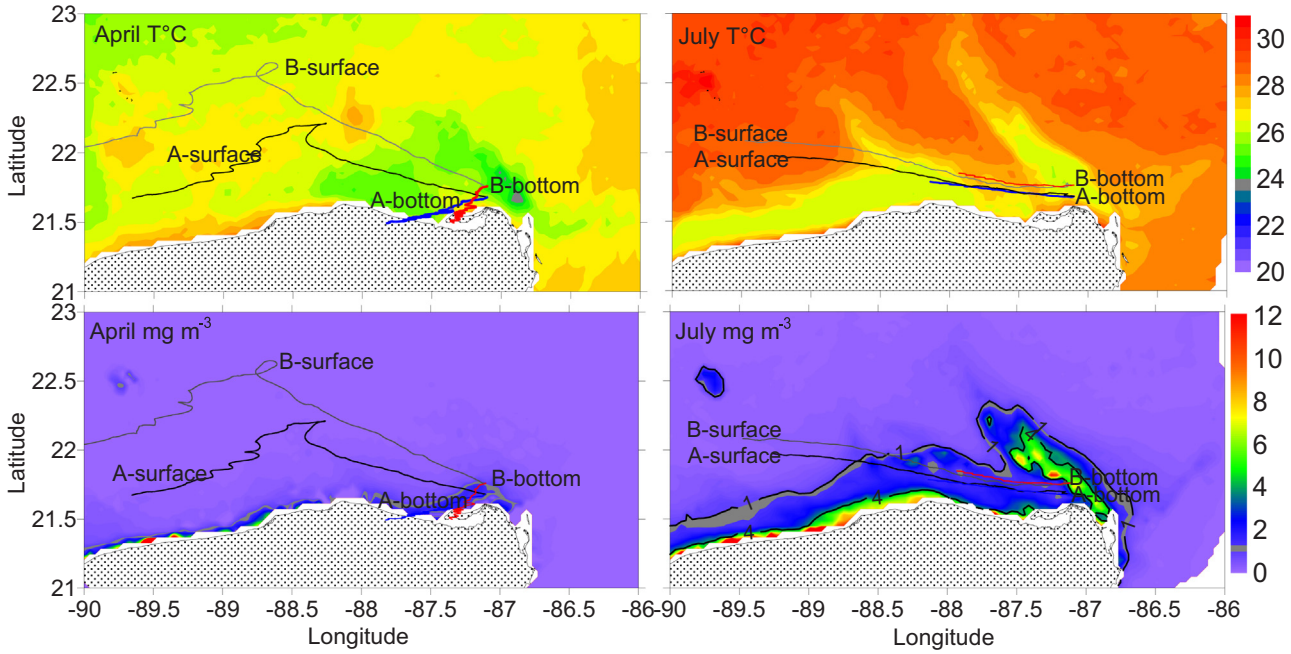


**Fig. 7.** Progressive vector diagram for the surface (0.5 m depth, black and gray line) and bottom (1 m before seafloor, red and blue line), showing a displacement by advection at sites A and B for April and July; and contour base maps for sea surface temperature (T °C), and sea surface Chlorophyll-a (mg $m^{-3}$) from NOAA satellite data (Aqua Modis NPP. 0.025 degrees, 3-day composite, April 5, and July 19, 2012).

associate this with slope water intrusion over the Yucatan Shelf.

The progressive vector diagrams (PVD, Fig. 7) showed a coincidence between the spatial and temporal distribution with respect to satellite data. On April 5 the wind changed abruptly (Figs. 2b, and 3c, squall event) suppressing the flow of the upwelling plume (toward the northwest, Fig. 7 April), evident on the satellite temperature image around 87.5° longitude. Therefore, the PVD vector from the surface (Fig. 7 black and gray line) showed a difference in the displacement of its particles, which change direction from northwestward to southwestward, around 88.7° (displacement site B) and 88.3° (displacement site A) longitude. The difference in spatial results is due to the flow diminishing by water friction, which PVD analysis cannot calculate spatially. However, the PVD vectors from the bottom (1 m before seafloor, Fig. 7, April blue and red line) always flowed southward (toward the coast), indicating current shearing currents across the water column which cannot be detected by satellite images, that shearing was clear in the profile currents (Fig. 4c, g). In July, the satellite image showed the upwelling plume flowing northwestward (offshore) associated with Chl-a (Fig. 7, July), while the PVD vector showed a constant flow westward (longshore) at both sites and levels associated with eastern wind advection (Fig. 3d).

### 3.5. Cross-shore distribution of the Chl-a

The statistics for the entire dataset from the CTD profiles from Chl-a showed statistical significance differences between campaigns (Kruskal-Wallis, $p = < 0.01$); the range of variation was 11.8 mg $m^{-3}$. Although the Chl-a mean value was lower in April than July, the maximums values were recorded in April. A summary of all CTD profile statistics is shown in Table 1. In April, Chl-a values of 1 mg $m^{-3}$ only reached the surface on April 5 and 6, around 15–17 km offshore, nevertheless, Chl-a values $>$ 1 mg $m^{-3}$ covered the bottom from April 2 to 11 around 18 to $>$ 20 km offshore (Fig. 8e), while on days 4, 5 and 6, high values ($>$ 11 mg $m^{-3}$) covered the bottom 12–16 km offshore. On the upwelling scenario was recorded with no phytoplankton bloom at surface and mid-layer (Fig. 8a, c). Temporally higher Chl-a was associated with a low temperature between April 4 and 5. In July, during the upwelling scenario, the Chl-a was lower than in April, with a maximum of 5.3 mg $m^{-3}$ at the bottom, but it was more dispersed across the shore, the isocline of 1 mg $m^{-3}$ reached the surface and mid-layer from 3 km offshore (Fig. 8b, d). During the not-upwelling scenario Chl-a values higher than 1 mg $m^{-3}$ were only recorded at the bottom between 8–14 and 18–20 km offshore (Fig. 8f), just in a couple days. On July 25, Chl-a values decreased below 1 mg $m^{-3}$ at the surface, while larger values were present at the bottom.

### 3.6. Anomaly analysis of temperature and Chl-a

In April, site A (8 km offshore) there is no anomalous inverse relation indicating a phytoplankton bloom due to AAY (Fig. 9, a). It is in site B (17 km offshore) that this inverse relationship occurs on days 2–4 (Fig. 9, b), however, AAY and Chl-a do not reach the surface (Figs. 5a, e, i, and 8a, c, e), remaining in the bottom layers (below 6 m). The increase in Chl-a on day 6 was due to the re-suspension of sediments due to the squall from that day. In the month of July is where the anomalies perfectly describe the inverse relationship between Bloom and Upwelling; at site A (8 km offshore, Fig. 9, c) on days 21 and 25 with the highest correlation coefficient obtained ($r = 0.81$); while that in site B (17 km offshore, Fig. 9d) is observed with a time lag regarding the shallow site (Site A), starting one day before the increase in phytoplankton. At least 3 different types of response of phytoplankton to the influence of AAY are identified, which are usually ephemeral in time and space, not necessarily observed on the surface, which makes it difficult to monitor. However, the RDA analysis statistically establishes the relation of cold water and increase of phytoplankton reinforcing the mean of that paper.

### 3.7. Temporal analysis of nutrients, Chl a and zooplankton biomass

During each campaign, two scenarios were characterized, upwelling (Up) and not-upwelling (Non-Up). The concentration of nitrate in April in the upwelling scenario (Fig. 10 a, Ap/Up) was significantly higher (Kruskal-Wallis, $p < 0.00$) with respect to the other scenarios. The ammonium concentration (Fig. 10b) was also significantly higher in the same month-scenario configuration with respect to the other three. The same was observed in the phosphate concentration (Fig. 10c), in

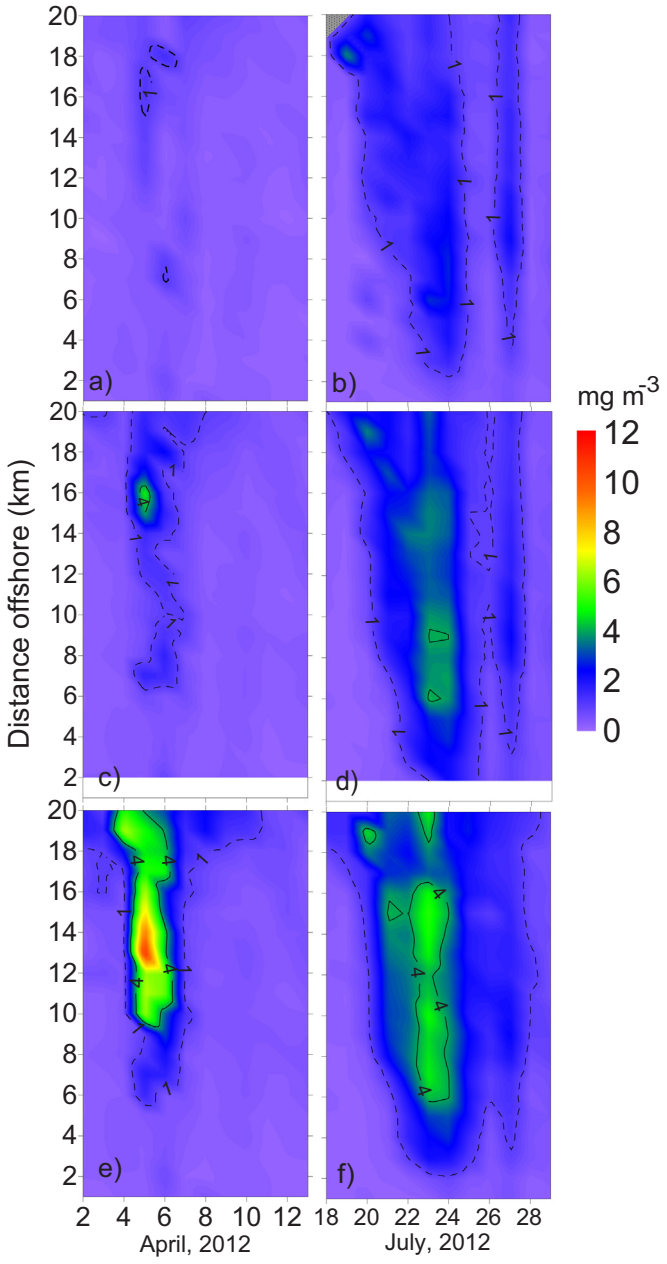


**Fig. 8.** Space-time diagram of Chl-a for data near the surface (0.5 m depth, a–b), mid layer (5 m depth, c–d), and near the bottom (1 m above the seafloor, e–f), April (left) and July (right).

addition, significant differences were observed with respect to the configuration of April/Non-Upwelling (Ap/Non-Up), which was lower with respect to the July/Non-Upwelling configuration (Ju/Non-Up). In the silicate concentration (Fig. 10d), significant differences were observed among other configurations, however, the Ap/Up configuration was always higher than the others. Nitrogen in its new and assimilated form, phosphate and silicate during the upwelling scenario in the month of April, turned out to be significantly higher than in July. On the other hand, the concentration of Chl-a (Fig. 10e) in July/Upwelling (Ju/Up) was significantly higher (Kruskal-Wallis, $p < 0.01$) than that of April, despite the maximum records of this variable in this month. Finally, the zooplankton showed the highest concentration significantly in the April/Non-Upwelling configuration as expected due to the peak of trophic lag.

### 3.8. Integration analysis of physical, chemical and biological components

First, Detrend Canonical Analysis (DCA) was conducted, which resulted with a gradient length from the ranking axes ≥ 2, which indicated a linear gradient distribution rather than unimodal, concluding in the use of the RDA (Ter-Braak and Smilauer, 1998).

#### 3.8.1. Redundancy Analysis (RDA) to april field campaign

The results of the Redundancy Analysis (RDA) carried out at site A (Fig. 11 a), indicated that the first axis explains 46.9% of the percentage of the cumulative variance and was not significant ($F = 4.5$, $p = 0.13$) according to the Monte Carlo test. The second axis explained 22.6% and neither axis was significant ($F = 1.51$ and $p = 0.07$). However, the correlation matrix showed a negative (positive) association of temperature (-0.82), density, (0.80) with nutrients. That means low temperature and high density were associated with increasing nutrients (NO3, NH4, SIO4, PO4). Likewise, the co-variable day 6 (D6)" presented a positive association between turbidity (0.60) and Chl-a, which means increasing in both variables at that day. The RDA explained 66% of the total variation.

Meanwhile, in site B (Fig. 11 b), the first axis explained 50.2% of the cumulative variance and was significant ($F = 6.2$, $p = 0.01$) according to the Monte Carlo test. The second axis explained 16.2%, and all axes were statistically significant ($F = 2.8$, $p = 0.001$). The correlation matrix indicated a negative association between temperature (T, − 0.58) with nutrients (NO3, NH4, SIO4, PO4) and Chl-a (CLA), which indicated that low temperature was associated with high nutrients and phytoplankton biomass. Positive associations at the co-variables day 4 (0.49) and day 5 (0.71) were also obtained, temporally associated to the maximum upwelling day and the squall day, respectively. The RDA analysis explained 81% of the total variation.

#### 3.8.2. Redundancy Analysis (RDA) to july field campaign

The RDA carried out in site A (Fig. 12 a) indicated that the first and second canonical axis explained 38.6% and 29% of the percentage of cumulative variance respectively, with significant statistical value at the first ($F = 3.6$; $p = 0.01$), and for all axes ($F = 1.8$; and $p = 0.01$), according to the Monte Carlo permutation test. The correlation matrix showed a positive association between the co-variable day 18 (D18, 0.55) and the silicate (SIO4), as well as with the temperature (T, 0.64). The RDA analysis explained a total variation of 74%. The variables density and salinity got statistical collinearity, therefore, this month was used salinity (S), which showed the best adjusted at the analysis.

The results for site B (Fig. 12 b) indicated that the first and second canonical axis explained 45.7% and 18.7% of the cumulative variance respectively, with significant value at the first ($F = 4.4$, $p = 0.0004$), and for all axes ($F = 1.7$, $p = 0.02$) according to the Monte Carlo test. The correlation matrix indicated a negative association between temperature (T, − 0.60) and silicate (SIO4), this last one nutrient had also a positive correlation with salinity (S, 0.50) and the co-variable day 19 (D19, 0.65). This relationship was associated with the entry of cold water and high-density water masses.

## 4. Discussion

In base to the results, we have enough evidence to determine that the slope water intrusion pulses create phytoplankton bloom events for a period of days, and spatially has implications closer to the shore. The main evidence was the temporal association between physical (temperature and density) and biological variables (Chl-a). During the study period, the temperature time series dropped below 22.5 °C six times and on two occasions it was possible to study and describe it in association with upwelling waters (Figs. 2a, 3). In these occasions, the wind shows a variability temporally associated to the slope water intrusion, as also as, the profile currents (Fig. 4), which showed this temporal variability alternating its direction in the zonal and meridional components.

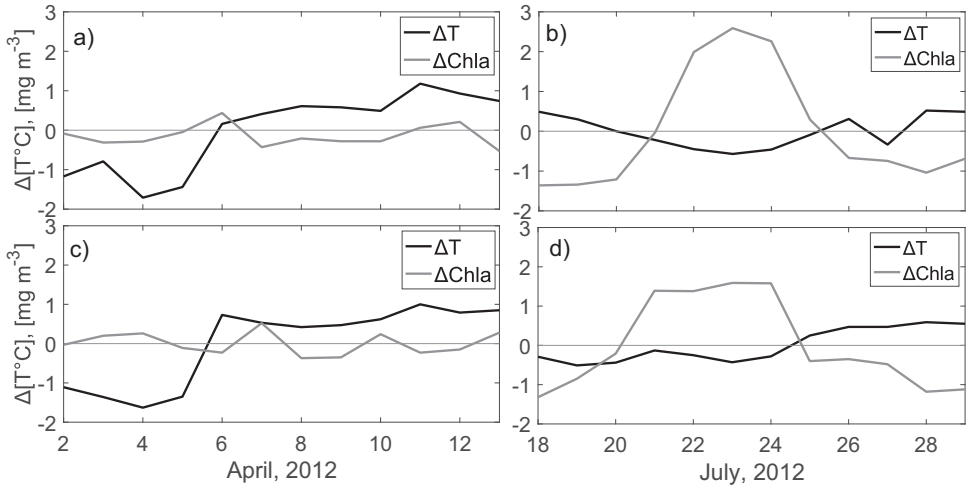


**Fig. 9.** Anomaly analysis of temperature (ΔT) and Chl-a (ΔChla) of the data recorded and collected at the *Sechii* disk depth, on sites A and B.

Spatially the evidence was the distribution of the slope water intrusion cross-shore (Figs. 5, 6, 8) on days when the upwelling was more intense, as also, the Caribbean Surface Waters distribution on Non-Upwelling period. By plotting satellite data during both field campaigns (Fig. 7) it was possible to observe the steady upwelling plume at the surface, (low temperature and high Chl-a). It is possible that the other four drops in temperature time series (Fig. 2a) were also upwelling events, considering that sea of the Caribbean basin and Yucatan Shelf surface-waters exceed 28 °C (Piñeiro et al., 2001; Pérez-Santos et al., 2010) and temperatures below 23 °C for shallow water masses from Cabo Catoche coast, have only been reported due to the intrusion of upwelling water from the Yucatan Channel or by ocean-atmosphere interaction in the winter (cold fronts) (Hernández-Télle et al., 1993, Pérez-Santos et al., 2010; Reyes-Mendoza et al., 2016). Finally, the nutrients concentration associated statistically to slope water intrusion, during specific days, was a strong evidence (RDA analysis).

### 4.1. Approaching the shoreline

At Cabo Catoche, during both field campaigns, a cross-shore gradient in temperature, salinity, density and Chl-a (Figs. 5 and 6) was observed, however, the YUW was closer to the shoreline in July (6 km offshore) than April (12 km offshore). During the April field campaign, the PVD vector from the bottom (1 m before seafloor) always flowed southward (toward coast), while the surface PVD flowed northwestward, indicating a shear in the water column, clearest on the current profiles (Fig. 4c, g). The wind advected the surface waters but not the deeper waters, which is where the YUW was present during the upwelling scenarios. In July, the PVD (Fig. 7) vector analysis showed a steady stream toward the north and west of the study site at both depths, roughly parallel to the north YP coast (< 15 m depth) and possibly these waters were advected by eastern winds (breezes).

The difference between Chl-a vertical distribution between field campaigns could be associated with buoyancy frequencies determined by the gradient density at the water column. In April upwelling scenario, the water column showed major gradient density associated to YUW respect to July, and therefore the buoyancy frequency was lower, trapping the Chl-a on mid and bottom layers, while on July the lower gradient density associated to YUW permitting high Chl-a distribution in all water column. Along the Australian coast (Roughan and Middleton, 2002), it appears that the cross-shore variation in upwelling water dispersion could be attributed to a combination of physical mechanisms. The wind stress (Ruiz Renteria, 1979; Pérez-Santos et al., 2010), the Yucatan current intensity and its spatial core variation along the east shore (Abascal et al., 2003; Ezer et al., 2003; Athie et al., 2011) are some of these mechanisms, even the bathymetric peak (Fig. 1c) in the study site could be a barrier to cold-bottom water approaching the shoreline (Fig. 5a). In that sense, on Fig. 13-i, is possible to observe

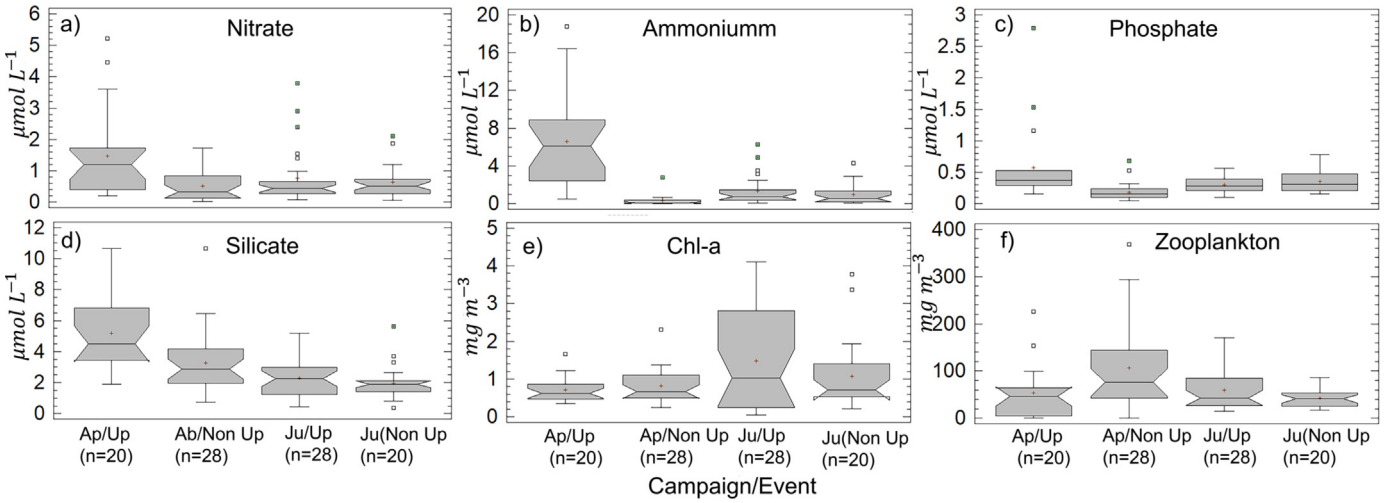


**Fig. 10.** Box plot analysis of a) nitrate, b) ammonium, c) silicate, d) phosphate, e) Chl-and f) zooplankton biomass classified by upwelling (Up) and non-upwelling (Non-Up) days to each field campaign (April, July) with n data.

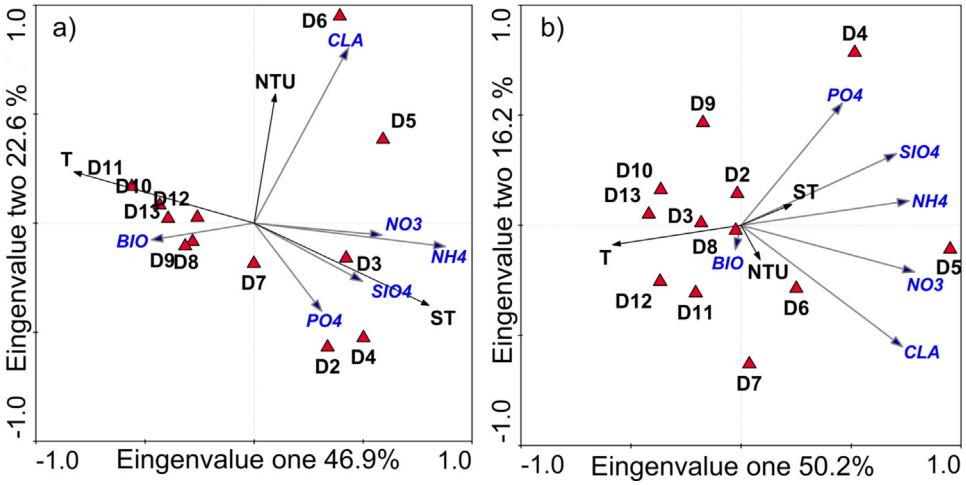


**Fig. 11.** Canonical redundancy analysis (RDA) with temperature (T), density (ST) and turbidity (NTU) as independent; nitrate (NO3), ammonium (NH4), silicate (SIO4), phosphate (PO4), chlorophyll-a (CLA) and zooplankton biomass as dependents (BIO); and sampling days (D) as a covariables (*Dummies*), for the month of April, in sites A (a) and B (b).

maximum Chl-a values trapped on the inner side of the barrier.

### 4.2. Nutrient inputs

The YUW has its own thermohaline characteristics and the nutricline is associated with the thermocline and pycnocline of the Yucatan Channel water column (Furnas and Smeyda, 1987; Merino, 1992; Carrillo et al., 2016). Therefore, it is possible to determine the origin of the nutrients arriving at the CC coast through the upwelling, the concentrations of which (Fig. 10) are mostly within the range reported for water masses from the whole of the YS (Furnas and Smayda, 1987; Merino, 1992, 1997) and coastal waters of CC (Reyes-Mendoza, 2010; Cárdenas-Palomo et al., 2015).

During the upwelling scenario, the mean nitrate and ammonium concentrations (Fig. 10a, c) along the CC coast is higher than in the absence of an upwelling event. Furthermore, the concentrations were higher in the upwelling scenario during April than in July. However, in July the phytoplankton biomass and its distribution were higher and more spread out in shallow waters (up to 4 km offshore) through more days. The relationship between nutrients and YUW was clear between variables and days (*dummy*) of major intensity of upwelling, how was observed on the Box-plot and RDA analysis, principally in site B for April and July. In upwelling waters and continental shelf seas, photosynthesis begins once Photosynthetically Active Radiation (PAR) is available allowing the phytoplankton to reduce the nitrate and phosphate in surface waters (Valiela, 1995; Williams and Follows, 2003; Simpson and Sharples, 2012). In that sense, the photosynthesis process could had begun previously on the euphotic zone at the Yucatan channel and keep developing throughout its track to the shelf and shallow waters from CC coast.

The difference in nutrient concentrations and phytoplankton biomass between field campaigns could be due to the onset of the upwelling season (around the end of March). Prior to July field campaign, there is evidence of three other upwelling events with three nutrient inputs and indications that low trophic levels may have been dynamic. The flow of energy through all trophic levels in the water column, including at the seafloor, creates great pelagic productivity in Cabo Catoche in the summer, as has been previously reported in several studies (Ramírez-Macías et al., 2012; Noyola et al., 2013; Cárdenas-Palomo et al., 2015, Licea et al., 2017).

Other nutrient inputs into these coastal waters could come from another source, for example sediment suspension by storm waves and turbulence (Pérez et al., 2000; Sharples et al., 2001; Hernández-Téllez et al., 1993), which could bring nutrients up from the bottom and reintroduce them to the water column. On April 6, NTU values (Fig. 5, d, h, i) were higher throughout the water column than on any other day due to turbulence generated by the northerlies event, however, the nutrient levels diminished at the start of this event. Finally, the input from the bottom by sediment suspension was not the main source of nutrients to the values reported here. Other source is the submarine groundwater discharge (SGD), which transports farm pesticides and wastewater with phosphorus and nitrogen above 50 μmol $L^{-1}$ (Aranda Cirerol et al., 2006; MutChler et al., 2007; Young et al., 2008) to the coastal waters and lagoon waters (Herrera-Silvera et al., 2004; Morales-Ojeda et al., 2010). The groundwater discharges are point sources and closer to the coast in the region (Aranda Cirerol et al., 2006; Hernández-

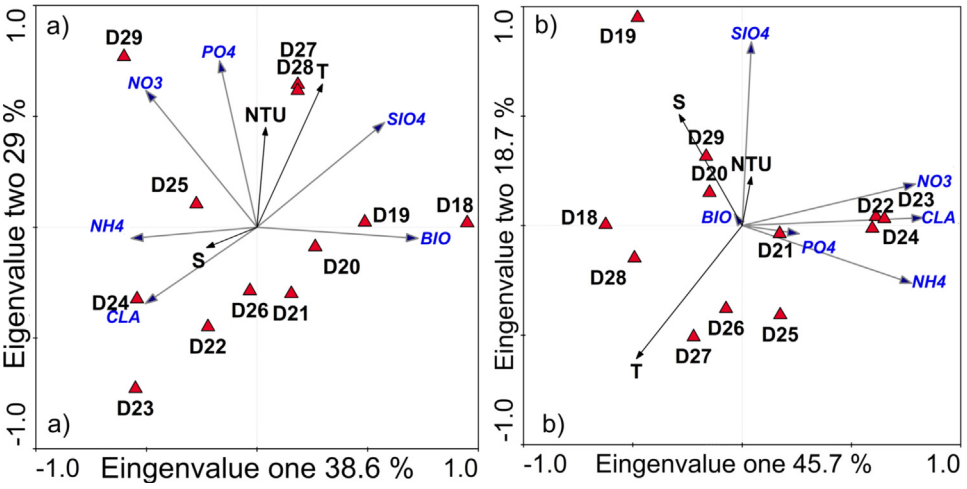


**Fig. 12.** Canonical redundancy analysis (RDA) with temperature (T), density (ST) and turbidity (NTU) as independent; nitrate (NO3), ammonium (NH4), silicate (SIO4), phosphate (PO4), chlorophyll-a (CLA) and zooplankton biomass as dependents (BIO); and sampling days (D) as a covariables (*Dummies*), for the month of July, in sites A (a) and B (b).

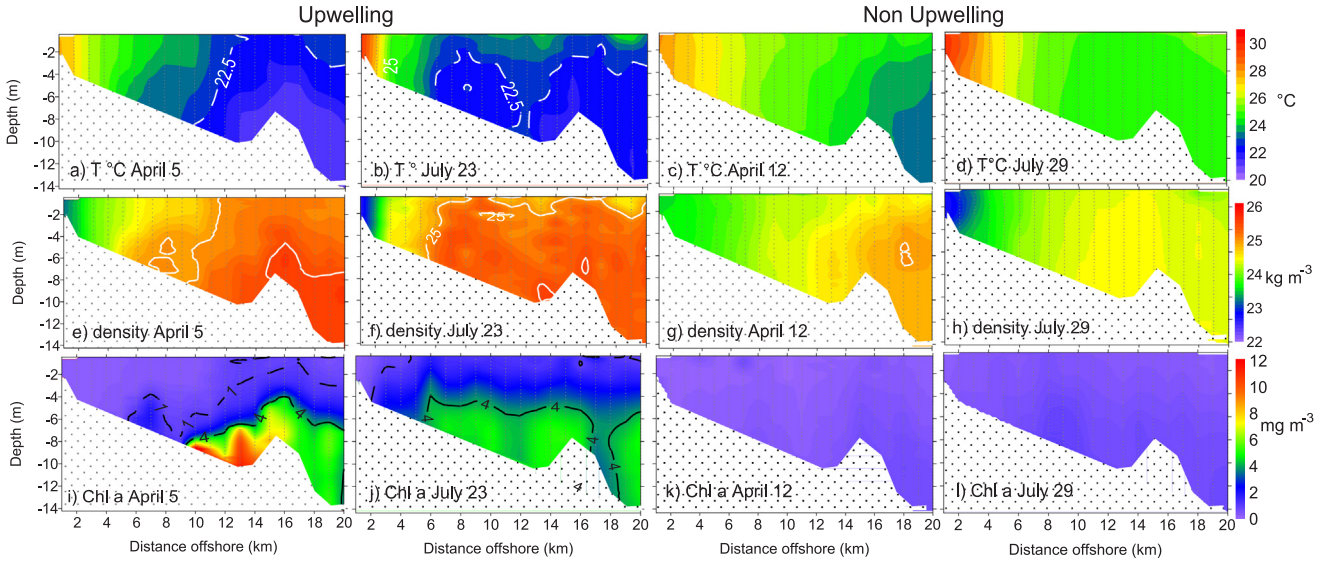


**Fig. 13.** Vertical profiles at the cross-shore transect of temperature (a–d), density (e–h) and Chl-a, (i–l) on April 5 and July 22 (upwelling example), and April 12 and July 29 (Non-Upwelling example).

Téllez et al., 1993; Null et al., 2014), hence they are unlikely to be the main source of nutrients in the present study, furthermore, the nutrients recorded were temporally associated with the YUW during the upwelling scenario in April and July. Silicate could be used as an indicator to identify nutrient runoff from the coast (Avelar et al., 2013), however, in April and July, the highest concentration of silicate was temporally associated with cold water at offshore sites (Fig. 10, d). Therefore there is no evidence of additional nutrient inputs mixing with the slope water intrusion unless this occurred initially.

### 4.3. Phytoplankton Bloom

At this point, is clear that the phytoplankton bloom is associated with upwelling (slope water intrusion) at Cabo Catoche. However, the temporal duration of this interactions are short periods, only a few days, therefore, it transforms them into ephemeral processes, which are difficult to detect and not always are evident on the surface to be studied via satellite. In Eastern Boundary Upwelling Systems (EBUS), Bakun (1996) suggested that following an upwelling event there is a quiescent period of around 10 days and that a calm period of 5 days or longer is enough to promote biological activities. Nieblas (2009) described these calm periods and the biological activity for the Non-EBUS off southeastern Australia and found evidence of an association between cold water and high Chl-a concentrations. In this study, Chl-a concentration was clearly associated with the coldest water recorded. Contrary to the findings of Bakun (1996) for the EBUS, the sequence wind – cold water - phytoplankton bloom does not strictly occur in this Non-EBUS. Naturally, on the continental shelf and shallow waters, the interactions are more complex than in the open sea, therefore the biogeochemical cycles are more dynamic and interactive over several trophic levels (Simpson and Sharples, 2012). Chl-a values ranged from 1 to 12 mg $m^{-3}$ (maximum values) during the first four days of the April field campaign, around 3 mg $m^{-3}$ $d^{-1}$. Then, on April 6, the "squall" generated turbulence, sediment suspension (lithic and biogenic solids) and turbidity throughout the entire water column (Fig. 5, d, h, i). Therefore high chlorophyll (> 6 mg $m^{-3}$) that day (D6) was not associated with the YUW (Fig. 11 a), this value must be associated with benthic diatoms more than pelagic diatoms, or even diatom floccules captured by the fluorimeter (CTD) (Miller, 2004), in accordance with processes reported on continental shelf seas (Jones and Halper, 1981; Darrow et al., 2003). Hence, the biological production during the April field campaign was a mixture of a bloom and advection. The zooplankton biomass was consistent with the expected results; the highest concentration was associated with warm waters, after upwelling and the phytoplankton bloom. In this study, although Chl a does not have conservative properties, using the current temporal resolution it was possible to detect an association with the YUW and follow the bloom's evolution.

### 4.4. Slope water intrusion

A conceptual idea to explain the physical-biological interactions on the Yucatan Shelf, could be, that uplifting of cold, high-nutrients water started in the Yucatan channel, where depths of 220–250 m can be reached (around Cozumel Island, in base Merino, 1992), and there the shelf edge diverges from the eastern shoreline. The cold, high-nutrient water reaches the euphotic zone and fuels the phytoplankton, and this will Bloom quickly (phytoplankton maximal growth rate at least of 1.5 $d^{-1}$, Darrow et al., 203) but it will not be evident at the surface, until the slope water intrusion reached the shallow waters from Cabo Catoche by buoyancy forcing (no more than Rosby radio ~ 10–30 km) of the SUW or of the Tropical Atlantic Central Water (TAC). Furthermore, the easterly wind could be stacking up this upwelled water by current advection and/or wind advection as has been proposed by Enriquez and Mariño-Tapia (2014). Despite the fact that the mechanisms causing the upwelling are physical in the Yucatan channel, over the YS along the CC coast, the chemical and biological implications can also be observed, mainly regarding primary production (Merino, 1992, 1997; Okolodkov, 2003; Pérez-Santos et al., 2010; Salmerón-García et al., 2011).

Based on Merino (1997), the estimated time for the cold, rich-nutrient water to reach the north of the YS as slope water intrusions is around 46–139 h from its origin. The results of the present study show the highest Chlorophyll concentration occurring with the coldest, most nutrient-rich water. This was evident on the Upwelling and Not-Upwelling scenario (Fig. 13), where was identified a gradient cross-shore confirmed by upwelling waters (YUW) and Caribbean surface water masses (CSW) in Cabo Catoche waters. This has also been reported previously (Furnas and Smeyda, 1987; Merino, 1997; Okolodkov, 2003, Licea et al., 2017).

### 4.5. Global ocean considerations

Global ocean temperatures have increased during the twentieth century and are expected to continue to rise with climate change

(Stocker et al., 2013). The sea surface temperature is warming and will propagate down through the water column and increase thermal stratification, ocean acidification and ocean deoxygenation, which will cause substantial changes in the physical, chemical and biological environment that will then affect the ocean's biogeochemical cycles and ecosystems in ways that we are only beginning to fathom (Gruber, 2011). In the EBUS system which has been more widely studied, there is little confidence regarding the future effects of climate change on coastal temperatures and biogeochemistry due to uncertainty in the countervailing responses to increased upwelling and coastal warming, the latter of which could increase thermal stratification and render upwelling less effective in lifting nutrient-rich deep waters into the photic zone (García-Reyes et al., 2015). The Non-EBUS has been studied less than the EBUS, as has the effect of climate change, however, similitudes with EBUS would be expected regarding the biogeochemical cycles, due to a reduction in nutrients.

In most studies of the physical and biological interactions, upwelling statistics are calculated over a large time scales (a month, season or years), whereas upwelling naturally occurs over short time scales (days to weeks), (García-Reyes et al., 2014). While our field design sacrifices some of the horizontal-spatial resolution by measuring a profile cross-shore, it has extensive benefits since it allows the evolution of the processes occurring in the water column to be followed, a component that previous studies (Furnas and Smayda, 1987; Merino, 1997) have not considered. Nevertheless, biogeochemical cycles are complex and in the pelagic zone could be considered ephemeral, as the temporal results of this study show, since reactions can occur in a matter of hours or in a couple of days. Therefore, if the temporal and spatial scale are not appropriate, it is difficult to explain or understand ecosystem function. Even in the EBUS, the spatiotemporal resolution of the data is a problem when attempting to resolve the effect of climate change on the ecosystem and its resiliency (García-Reyes et al., 2015).

## 5. Conclusions

The Non-EBUS from Yucatan, through slope water intrusion pulses create phytoplankton bloom events for a period of days, and spatially has implications nearer to the Cabo Catoche shore. In an upwelling scenario, the ranges of the variables are characterized by temperatures around 19.6–22.5 °C, salinities from 35.5 to 37, densities of 25–26 kg $m^{-3}$ and chlorophyll around 1–5.3 mg $m^{-3}$. However, the temporal duration of the physical-biological interactions is by short periods, only a few days, therefore, it transforms them into ephemeral processes and not always are evident on the surface, therefore they are difficult to study and describe. It is very important to study the coupled physical-biological processes, due that help to understand the enhancing on the productivity and how triggering the energy flow at the pelagic ecosystem. The slope water intrusion has considerable biological implications on the Cabo Catoche coast and all the north coast of the Yucatan Peninsula due its distribution long shore.

## Acknowledgements

Fondo Sectorial CONACYT-Secretaría de Energía-Sustentabilidad Energética 2015-2016, for the postdoctoral scholarship awarded on behalf of the author. As also to partial funding from proyects: Fomix Conacyt-Yucatán (No. 018897), Análisis de las causas, dispersión y consecuencias ambientales de la marea roja en Yucatán. The study was also supported by the Laboratorio de Procesos Costeros y Oceanografía Física (LAPCOF) and Laboratorio de Producción Primaría (LPP) of the Centro de Investigación y de Estudios Avanzados del IPN, Unidad Mérida, and Dr. David Valdes who granted meteorological data. We also thank to Dr. Marisol Garcia-Reyes and Cristina Torres for her scientific suggestions per this work; Emanuel Uc Sanchez, Natali Cardenas and Francisco Puc for technical assistance; Ileana Osorio Moreno for assistance in laboratory analysis.

## References

Abascal, a.J., Sheinbaum, J., Candela, J., Ochoa, J., Badan, A., 2003. Analysis of flow variability in the Yucatan channel. J. Geophys. Res. 108, 3381. https://doi.org/10.1029/2003JC001922.

Aranda Cirerol, N., Herrera-Silveira, J.a., Comín, F.a., 2006. Nutrient water quality in a tropical coastal zone with groundwater discharge, northwest Yucatán, Mexico. Estuar. Coast. Shelf Sci. 68, 445–454. https://doi.org/10.1016/j.ecss.2006.02.015.

Ardisson, P.L., May-Kú, M.A., Herrera-Dorantes, M.T., Arellano-Guillermo, A., 2011. El Sistema Arrecifal Mesoamericano-México: consideraciones para su designación como Zona Marítima Especialmente Sensible. Hidrobiologica 21, 261–280.

Athie, G., Candela, J., Sheimbaun Julio, Badan, A., Ochoa, J., 2011. Yucatan Current variability through the Cozumel and Yucatan channels. Cienc. Mar. 37, 471–492.

Avelar, M., Bonilla-Heredia, B., Merino-Ibarra, M., Herrera-Silveira, J.A., Ramirez, J., Rosas, H., Valdespino, J., Carricart-Ganivet, J.P., Martínez, A., 2013. Iron, cadmium, and chromium in seagrass (*Thalassia testudinum*) from a coastal nature reserve in karstic Yucatan. Environ. Monit. Assess. 185, 7591–7603. https://doi.org/10.1007/s10661-013-3121-7.

Cadena-Ramírez, J.L., 2013a. Procedimiento para recolectar zooplancton con red Bongo durante la campaña oceanográfica FU1201-284. Serie Embarcaciones Oceanográficas, CICESE. Informe Técnico CICESE No. 106453. Centro de Investigación Científica y de Educación Superior de Ensenada, Baja California, pp. 29.

Cadena-Ramírez, J., 2013b. Procedimiento para recolectar zooplancton con red Bongo durante la.

Cárdenas-Palomo, N., 2007. Distribución espacio-temporal de variables hidrobiológicas asociadas con el uso del hábitat del tiburón ballena (Rhincodon typus) en el noreste de la Península de Yucatán (Tesis de Maestría). Centro de Investigación y de Estudios Avanzados del IPN, pp. 86.

Cárdenas-Palomo, N., Herrera-Silveira, J., Velázquez-Abunader, I., Reyes, O., Ordoñez, U., 2015. Distribution and feeding habitat characterization of whale sharks Rhincodon typus in a protected area in the north Caribbean Sea. J. Fish Biol. 86, 668–686. https://doi.org/10.1111/jfb.12589.

Carlson, D.F., Muscarella, P.A., Gildor, H., Lipphardt, B.L., Fredj, E., 2010. How useful are progressive vector diagrams for studying coastal ocean transport? Limnol. Oceanogr. Methods 8, 98–106. https://doi.org/10.4319/lom.2010.8.0098.

Carrillo, L., Johns, E.M., Smith, R.H., Lamkin, J.T., Largier, J.L., 2016. Pathways and hydrography in the Mesoamerican Barrier Reef System Part 2: water masses and thermohaline structure. Cont. Shelf Res. 120, 41–58. https://doi.org/10.1016/j.csr.2016.03.014.

Cerdeira-Estrada, S., López-Saldaña, G., 2011. A novel satellite-based ocean monitoring system for Mexico Nuevo Sistema Satelital de Monitoreo Oceánico para México. Cienc. Mar. 37, 237–247.

Chavez, F.P., Messié, M., 2009. A comparison of eastern boundary upwelling ecosystems. Prog. Oceanogr. 83, 80–96. https://doi.org/10.1016/j.pocean.2009.07.032.

Cochrane, J.D., 1968. Currents and Waters of the Eastern Gulf of Mexico and Western Caribbean, of the Western Tropical Atlantic Ocean, and of the Eastern Tropical Pacific Ocean (Technical Report No. 68-8T). TAMU, Houston, Texas, pp. 19–28.

Coelho-souza, S.A., López, M.S., Guimarães, J.R.D., Coutinho, R., Candella, R.N., 2012. Biophysical interactions in the Cabo Frio upwelling systems Southeastern Brazil. Braz. J. Oceanogr. 60, 353–365. https://doi.org/10.1590/S1679-87592012000300008.

Darrow, B.P., Walsh, J.J., Vargo, G.a., Masserini, R.T., Fanning, K. a., Zhang, J.-Z., 2003. A simulation study of the growth of benthic microalgae following the decline of a surface phytoplankton bloom. Cont. Shelf Res. 23, 1265–1283. https://doi.org/10.1016/S0278-4343(03)00130-4.

Emery, W.y., Thomson, R., 1997. Data Analysis Methods in Physical Oceanography. Elsevier, USA, pp. 638.

Enriquez, C., Mariño-Tapia, I.J., Herrera-Silveira, J.a., 2010. Dispersion in the Yucatan coastal zone: implications for red tide events. Cont. Shelf Res. 30, 127–137. https://doi.org/10.1016/j.csr.2009.10.005.

Enriquez, C.E., Mariño-Tapia, I., 2014. Mechanisms driving a coastal dynamic upwelling. In: Proceedings of the 17th Physics of Estuaries and Coastal Seas (PECS) Conference. Porto de Galinhas, Pernambuco, Brazil, pp. 17–20.

Ezer, T., Oey, L.-Y., Lee, H.-C., Sturges, W., 2003. The variability of currents in the Yucatan channel: analysis of results from a numerical ocean model. J. Geophys. Res. 108, 3012. https://doi.org/10.1029/2002JC001509. (C1).

Furnas, M.J., Smayda, T.J., 1987. Inputs of subthermocline waters and nitrate onto the Campeche Bank. Cont. Shelf Res. 7, 161–175. https://doi.org/10.1016/0278-4343(87)90077-X.

García-Reyes, M., Sydeman, W.J., Schoeman, D.S., Rykaczewski, R.R., Bryan, B.A., J, S.A., Steven, B.A., 2015. Ecosystems under pressure: climate change, upwelling, and eastern boundary upwelling ecosystems. Front. Mar. Sci. 1–10. https://doi.org/10.3389/fmars.2015.00109.

García-Reyes, M., Largier, J.L., Sydeman, W.J., 2014. Synoptic-scale upwelling indices and predictions of phyto- and zooplankton populations. Prog. Oceanogr. 120, 177–188. https://doi.org/10.1016/J.POCEAN.2013.08.004.

Gong, G.-C., Shiah, F.-K., Liu, K.-K., Wen, Y.-H., Liang, Ming-Hsin, 2000. Spatial and temporal variation of Chlorophyll a, primary productivity and chemical hydrography in the southern East China Sea. Cont. Shelf Res. 20, 411–436. https://doi.org/10.1016/S0278-4343(99)00079-5.

Gruber, N., 2011. Warming up, turning sour, losing breath: ocean biogeochemistry under global change. Philos. Trans. R. Soc. A Math. Phys. Eng. Sci. 369, 1980–1996. https://doi.org/10.1098/rsta.2011.0003.

Hernández -Téllez, J., Aldeco, J., Salas-de-León, D.A., 1993. Cooling and heating due to latent and sensible heat over the Yucatan continental shelf. Atmósfera 6 (4),

223–233.
Herrera-Silvera, J.A., Comin, F., Aranda-Cirerol, N., Troccoli, L., y Capurro, L., 2004. Coastal water quality assessment in the Yucatan Peninsula: management implications. Ocean Coast. Manag. 47 (11), 625–639.
Holmes, W.R., 1970. The Secchi disk in turbid coastal waters. Limnol. Oceanogr. 15, 688–694.
Jones, B.H., H, D., 1981. Biological and physical aspects of a coastal upwelling event observed during March–April 1974 off northwest Africa*. Deep Sea Res. 28A, 71–81.
Jouanno, J., Pallàs-Sanz, E., Sheinbaum, J., 2018. Variability and dynamics of the Yucatan upwelling: high resolution simulations. J. Geophys. Res. Ocean 1–25. https://doi.org/10.1002/2017JC013535.
Lara-Lara, J.R., 2008. Los ecosistemas marinos, en Capital natural de México, vol. I: Conocimiento actual de la biodiversidad. CONABIO, México, pp. 135–159.
Licea, S., Luna, R., Okolodkov, Y., Cortés-Altamirano, R., 2017. Phytoplankton abundance and distribution on the Yucatan shelf (June 1979 and April 1983). Новости сист. низш. раст. — Nov. Sist. Nizsh. Rast. 51, 121–144.
Medina-Gómez, I., Herrera-Silveira, J.a., 2006. Primary production dynamics in a pristine groundwater influenced coastal lagoon of the Yucatan Peninsula. Cont. Shelf Res. 26, 971–986. https://doi.org/10.1016/j.csr.2006.03.003.
Merino, I.M., 1992. Afloramiento en la Plataforma de Yucatán. Estructura y Fertilización (Tésis de Doctorado). UNAM-Instituto de Ciencias del Mar y Limnología, México DF, pp. 254.
Merino, M., 1997. Upwelling on the Yucatan Shelf: hydrographic evidence. J. Mar. Syst. 13, 101–121. https://doi.org/10.1016/S0924-7963(96)00123-6.
Merino-Virgilio, F. del C., Okolodkov, Y.B., Aguilar-Trujillo, A.C., Osorio-Moreno, I., Herrera-silveira, J.A., 2014. Florecimientos algales nocivos en las aguas costeras del norte de Yucatán (2001–2013). In: Golfo de México. Contaminación E Impacto Ambiental: Diagnóstico Y Tendencias. p. 1174.
Miller, 2004. Biological Oceanography. Blackwell Publishing, USA, pp. 401.
Mitchell-Innes, B.A., Richardson, A.J., Painting, S.J., 1999. Seasonal changes in phytoplankton biomass on the western Agulhas Bank, South Africa. S. Afr. J. Mar. Sci./S. -Afr. Tydskr. Seewet 7615, 217–233. https://doi.org/10.2989/025776199784125872.
Morales-Ojeda, S.M., Herrera-Silveira, J.a., Montero, J., 2010. Terrestrial and oceanic influence on spatial hydrochemistry and trophic status in subtropical marine nearshore waters. Water Res. 44, 5949–5964. https://doi.org/10.1016/j.watres.2010.07.046.
MutChler, T., Dunton, K.H., Townsend-Small, A., Fredriksen, S., Rasser, M.K., 2007. Isotopic and elemental indicators of nutrient sources and status of coastal habitats in the Caribbean Sea, Yucatan Peninsula, Mexico. Estuar. Coast. Shelf Sci. 74 (3), 449–457.
Nieblas, Anne-Elise, Sloyan, B., Hobday, A., Coleman, R., Richardson, A., 2009. Variability of biological production in low wind-forced regional upwelling systems: a case study off southeastern Australia. Limnol. Oceanogr. 54 (5), 1548–1558.
Noyola, J., Mascaró, M., Caamal-Monsreal, C., Noreña-Barroso, E., Díaz, F., Re, D., Sánchez, A., Rosas, C., 2013. Effect of temperature on energetic balance and fatty acid composition of early juveniles of Octopus maya. J. Exp. Mar. Biol. Ecol. 445, 156–165. https://doi.org/10.1016/j.jembe.2013.04.008.
Null, K.A., Knee, K.L., Crook, E.D., de Sieyes, N.R., Rebolledo-Vieyra, M., Hernández-Terrones, L., Paytan, A., 2014. Composition and fluxes of submarine groundwater along the Caribbean coast of the Yucatan Peninsula. Cont. Shelf Res. 77, 38–50. https://doi.org/10.1016/j.csr.2014.01.011.
Okolodkov, Yuri B., 2003. A review of Russian plankton research in the Gulf of Mexico and the Caribbean Sea in the 1960–1980s. Hidrobiológica 13 (3), 207–221.
Omori, M.y.T., Ikeda, 1984. Methods in Marine Zooplankton Ecology. J. Wiley & Sons, N. York, pp. 332.
Parsons, T., Maita, Y., Lally, y.C., 1984. A Manual of Chemical and Biological Methods of Seawater Analysis. Pergamon Press, Oxford, pp. 173.
Pereira Brandini, F., Nogueira, M., Simião, M., Carlos Ugaz Codina, J., Almeida Noernberg, M., 2013. Deep Chlorophyll maximum and plankton community response to oceanic bottom intrusions on the continental shelf in the South Brazilian Bight. Cont. Shelf Res. 89, 61–75. https://doi.org/10.1016/j.csr.2013.08.002.
Pérez, B.C., Day, J.W., Rouse, L.J., Shaw, R.F., Wang, M., 2000. Influence of Atchafalaya River discharge and winter frontal passage on suspended sediment concentration and flux in Fourleague Bay, Louisiana. Estuar. Coast. Shelf Sci. 50, 271–290. https://doi.org/10.1006/ecss.1999.0564.
Pérez-Santos, I., Schneider, W., Sobarzo, M., Montoya-Sánchez, R., Valle-Levinson, A., Garcés-Vargas, J., 2010. Surface wind variability and its implications for the Yucatan basin-Caribbean Sea dynamics. J. Geophys. Res. 115, C10052. https://doi.org/10.1029/2010JC006292.
Piñeiro, R., Giménez, E., Moreno, V., Burgos, R., Betanzos, a., 2001. Características térmicas del Banco de Campeche. Cienc. Pesq. 14, 83–87.
Ramírez-Macías, D., Vázquez-Haikin, a., Vázquez-Juárez, R., 2012. Whale shark Rhincodon typus populations along the west coast of the Gulf of California and implications for management. Endanger. Species Res 18, 115–128. https://doi.org/10.3354/esr00437.
Reyes-Mendoza, 2010. Caracterización espacial y temporal de la columna de agua en la Reserva de la Biosfera del Tiburón Ballena (Rhincodon typus) ubicada al noreste de la Península de Yucatán (Tesis de Maestría). CINVESTAV-IPN, pp. 110.
Reyes-Mendoza, O., Mariño-Tapia, I., Herrera-Silveira, J., Ruiz-Martinez, G., Enriquez, C., Largier, J.L., 2016. The effects of wind on upwelling off cabo catoche. J. Coast. Res. 32 (3), 638–650.
Roughan, M., Middleton, J.H., 2002. A comparison of observed upwelling mechanisms off the east coast of Australia. Cont. Shelf Res. 22, 2551–2572. https://doi.org/10.1016/S0278-4343(02)00101-2.
Roughan, M., Oke, P.R., Middleton, J.H., 2003. A modeling study of the climatological current field and the trajectories of upwelled particles in the East Australian current. J. Phys. Oceanogr. 33, 2551–2564. https://doi.org/10.1175/1520-0485(2003)033<2551:AMSOTC>2.0.CO;2.
Ruiz Renteria, F.G., 1979. Upwelling North of the Yucatan Peninsula (M.S. Thesis). Dept. of Oceanography, Texas A&M University, Texas, pp. 92.
Ruiz-Castillo, E., Gomez-Valdes, J., Sheinbaum, J., Rioja-Nieto, R., 2016. Wind-driven coastal upwelling and westward circulation in the Yucatan shelf. Cont. Shelf Res. 118, 63–76. https://doi.org/10.1016/j.csr.2016.02.010.
Salmerón-García, O., Zavala-Hidalgo, J., Mateos-Jasso y, A., Romero-Centeno, R., 2011. Regionalization of the Gulf of Mexico from space-time Chlorophyll-a concentration variability. Ocean Dyn. 61, 439–448.
Sharples, J., Moore, C.M., Abraham, E.R., 2001. Internal tide dissipation, mixing, and vertical nitrate flux at the shelf of NE New Zealand. J. Geophys. Res. 106 (C7), 14069–14081. https://doi.org/10.1029/2000JC000604.
Simpson, J.H., Sharples, s.J., 2012. Introduction to the Physical and Biological Oceanography of Shelf Seas. Cambridge, United Kingdom.
Strickland, J.D.H., y Parsons, T.R., 1972. A Practical Handbook of Seawater Analysis. Fisheries Research Board of Canada, Bulletin 167, 2nd Ed. The Alger Press Ltd, Ottawa, Canada, pp. 310.
Stocker, T.F., Qin, D., Plattner, G.-K., et al., 2013. Technical Summary. In: Stocker, T.F., Qin, D., Plattner, G.-K. (Eds.), Climate change 2013: the physical science basis. Contribution of working group I to the fifth assessment report of the intergovernmental panel on climate change. Cambridge University Press, Cambridge.
Ter Braak, C.J.F., Smilauer, P., 1998. CANOCO Release 4. Reference Manual and Users Guide to CANOCO for Windows: Software for Canonical Community Ordination. Microcomputer Power, Ithaca, USA.
Tomczak, M.y., Godfrey, S., 1994. Regional Oceanography An Introduction. Bluter and Tanner, Great Britain, pp. 382.
UNESCO, 1979. Zooplankton sampling. Monogr. Oceanogr. Methodol. 2, 174.
Valiela, I., 1995. Marine Ecological Processes, Sec. ed. Springer, USA, pp. 686.
Williams, R.G., Follows, M.J., 2003. Physical transport of nutrients and the maintenance of biological production. In: Fasham, M. (Ed.), Ocean Biogeochemistry: The Role of the Ocean Carbon Cycle in Global Change. Springer, Germany, pp. 19–51 (ISBN: 3-540-42398-2).
Young, Megan B., Gonneea, Meagan Eagle, Fong, Derek A., Moore, Willard S., Herrera-Silveira, Jorge, Paytan, Adina, 2008. Characterizing sources of groundwater to a tropical coastal lagoon in a karstic area using radium isotopes and water chemistry. Mar. Chem. 109 (3–4), 377–394.
Zavala-Hidalgo, J., Romero-Centeno, R., Mateos-Jasso, A., Morey, S.L., Martínez-López, B., 2014. The response of the Gulf of Mexico to wind and heat flux forcing: what has been learned in recent years? Atmosfera 27, 317–334. https://doi.org/10.1016/S0187-6236(14)71119-1.

## Further reading

Hernández-Terrones, L., Rebolledo-Vieyra, M., Merino-Ibarra, M., Soto, M., Le-Cossec, A., Monroy-Ríos, E., 2011. Groundwater pollution in a karstic region (NE Yucatan): Baseline nutrient content and flux to coastal ecosystems. Water. Air. Soil Pollut. 218, 517–528. https://doi.org/10.1007/s11270-010-0664-x.